

Cite this: *Chem. Commun.*, 2012, **48**, 6945–6947

www.rsc.org/chemcomm

COMMUNICATION

α -MnO₂ nanotubes: high surface area and enhanced lithium battery properties†

Lihong Li, Caiyun Nan, Jun Lu, Qing Peng* and Yadong Li*

Received 30th March 2012, Accepted 21st May 2012

DOI: 10.1039/c2cc32306k

A simple one-step route for preparing α -MnO₂ nanotubes is reported. The α -MnO₂ nanotubes exhibit a high surface area of 226 m² g⁻¹ and reversible capacity of 512 mA h g⁻¹ at a high current density of 800 mA g⁻¹ after 300 cycles, as well as cycling stability when measured as an anode in lithium batteries.

Manganese oxide (α -MnO₂) with 2 × 2 tunnels constructed from double chains of octahedral [MnO₆] structure, beneficial for Li⁺ transfer, has been studied as an anode for lithium batteries, owing also to its high storage capacity, low cost, environmental friendliness, and natural abundance.^{1–4} However, potential applications in practical lithium batteries are limited due to its poor electrical conductivity and large volume expansion during repeated lithium cycling processes.⁵ Herein we report the synthesis of α -MnO₂ nanotubes and their satisfactory lithium battery properties.

One-dimensional (1D) nanostructured morphologies of manganese oxide with small dimensional structures for efficient transport of electrons and controlled size have been designed to overcome the problems of manganese oxide when used as anode,^{6–9} because of their unique properties leading to improved performances.^{10–13} Our group had reported the synthesis of a series of one-dimensional (1D) single-crystal nanostructures of MnO₂ with different crystallographic structures, which provided the possibility of detecting the theoretical operating limits of a lithium battery.^{14–16} However, the high capacity could not be well retained after extended cycling.^{17–19} To retain or increase the high capacity, many efforts have been made to combine MnO₂ with graphene or nanotubes,^{20,21} which, however, are complex to prepare. In the study, we aimed at obtaining a MnO₂ material with high capacity *via* a simple fabrication method. To achieve high capacity, electrode materials can be modified as follows: (i) minimizing solid-state diffusion lengths for both Li⁺ and e⁻; (ii) introducing mesopore channels for substantial Li⁺ and e⁻ transfer; and (iii) amplifying the intrinsic surface area.

Large surface and thin-walled α -MnO₂ nanotubes thus seems a promising material. In our previous report, MnO₂ nanotubes were obtained by a multistep method, involving solid-state synthesis and scrolling the solid-state precursors.¹⁴ However, using such a multistep process, the solid-state precursors are not easy to be completely scrolled and large surface area nanostructured α -MnO₂ could not be obtained. Therefore, it is still a challenge to synthesize large surface α -MnO₂ thin nanotubes *via* a facile one-step method.

Herein we demonstrate a facile exfoliation and scrolling approach to fabricate α -MnO₂ nanotubes. We also increased the lithium storage capacity of MnO₂ with nanotube structure and large surface area, since the structure has nanosized walls (< 7 nm), which shortens the solid-state diffusion lengths for both Li⁺ and e⁻, along with mesopore channels (> 5 nm) and large total pore volume, which efficiently enable solvated Li⁺ transport. In the study, aqueous tetra(*n*-butyl)ammonium hydroxide (TBAOH) was added, which is considered as an effective agent to assist the exfoliation and scrolling of layered structure oxides.^{22,23} We demonstrated that large surface area α -MnO₂ nanotubes could be formed from δ -MnO₂ nanoflowers *via* the exfoliation and scrolling approach, and then demonstrated that the as-prepared mesostructured α -MnO₂ nanotubes were an effective anode material with greatly enhanced lithium storage properties, with a reversible capacity as high as 512 mA h g⁻¹ at a constant current density of 800 mA g⁻¹, even after 300 cycles.

The morphologies of the MnO₂ samples were characterized with increased reaction time by TEM and SEM images as shown in Fig. 1a–e and Fig. S1, S2†, respectively, which indicate that the reaction time is important in terms of the morphology. When the reaction time was less than 12 h, flower-like MnO₂ nanopowders were formed, the diameter of which grew from 150 to 300 nm with increased time. Meanwhile, from the HRTEM image (Fig. S3†) of MnO₂ nanoflowers treated with TBAOH for 12 h, it was found that the platelets tended to be exfoliated into thinner platelets. Further increasing the reaction time to 24 h, scrolling nanotubes began to form. From the HRTEM image (Fig. S4†) it was found that the tubes were connected at their ends to form long nanotubes. When the reaction time was longer than 48 h, long nanotubes of around 20 nm width and several micrometers length were observed from both TEM (Fig. 1e) and SEM images (Fig. 1f and S2e, f†). HRTEM analysis (Fig. 1g and S1c†)

Department of Chemistry, Tsinghua University, Beijing 100084, China. E-mail: pengqing@mail.tsinghua.edu.cn, ydli@mail.tsinghua.edu.cn; Fax: 86-10-6279-2798; Tel: 86-10-62772350

† Electronic supplementary information (ESI) available: Detailed experimental procedures, further TEM and SEM images, EDS, XRD patterns, XPS patterns and charge–discharge voltage profiles. See DOI: 10.1039/c2cc32306k

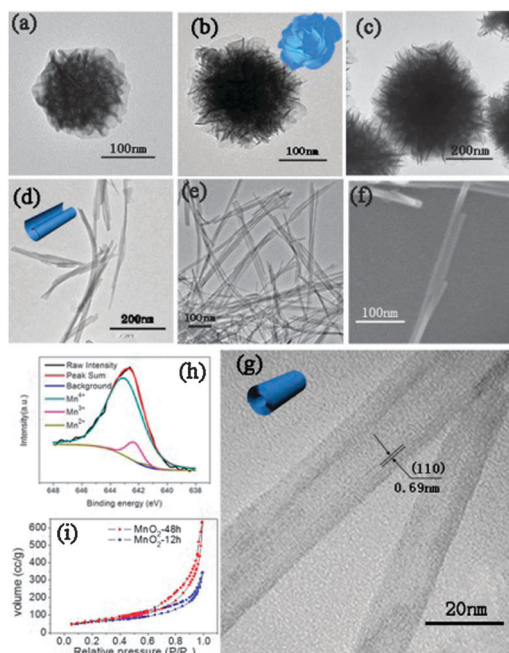


Fig. 1 Morphology evolution of MnO_2 from nanoflowers to nanotubes with different reaction times: TEM images of the products obtained for (a) 1, (b) 6, (c) 12, (d) 24 and (e) 48 h and (f) SEM after 48 h; (g) HRTEM image and (h) the fitted XPS spectra of $\text{Mn } 2p_{3/2}$ for the product at 48 h; (i) N_2 adsorption/desorption isotherms of products at 12 and 48 h.

provides more information about the nanotubes obtained for 48 h with nanosized walls (< 7 nm), which can minimize the solid-state diffusion lengths for both Li^+ and e^- , and shows the apparent lattice fringes of the crystal. The interlayer distance is calculated to be 0.69 nm, which agrees with the separation between the (110) planes of $\alpha\text{-MnO}_2$. X-Ray diffraction (XRD) patterns (Fig. S5†) confirm that the nanoflowers obtained at less than 12 h are the rhombohedral phase of $\delta\text{-MnO}_2$ (JCPDS no. 86-666) and the nanotube MnO_2 is tetragonal $\alpha\text{-MnO}_2$ (JCPDS no. 81-1947). The weak and broad diffraction peaks from MnO_2 indicate the nature of the nanocrystals.

The Mn XPS pattern of $\alpha\text{-MnO}_2$ nanotubes (Fig. S6†) showed two peaks located at 642.0 and 653.6 eV attributable to $\text{Mn } 2p_{3/2}$ and $\text{Mn } 2p_{1/2}$, respectively, with a spin-energy separation of 11.6 eV. The peak values are in good agreement with those reported for MnO_2 .²⁴ The fitted XPS spectra of $\text{Mn } 2p_{3/2}$ can be referenced to literature reports of 640.8 eV for Mn^{2+} , 641.7 eV for Mn^{3+} and 642.2 eV for Mn^{4+} ,²⁵ and demonstrate that Mn mainly exhibits 3+ and 4+ oxidation state (Fig. 1h and S7†), with a ratio of about 1 : 9. Furthermore, the EDS pattern (Fig. S8†) indicates the presence of K with a K/Mn atomic ratio around 0.1 in our sample, which is also confirmed by the XPS pattern of the sample. The K^+ concentration of MnO_2 in tunnel or layer structures has a dramatic influence on the magnetic properties,^{8,26} as also been found in our case and to be further studied. Based on the results of EDS and XPS, the average oxidation state of Mn is 3.9+. Fig. S9† shows the deconvoluted O 1s spectrum, where one sharp peak located at 529.4 eV and two broad peaks located at 530.5 and 531.9 eV can be observed. This spectrum

Table 1 Key parameters of MOT and MOF

Sample	t/h	$A_s/\text{m}^2 \text{g}^{-1}$	$V_p/\text{cm}^3 \text{g}^{-1}$	d_{av}/nm
MOF	12	204	0.53	3.8
MOT	48	226	0.97	7.8

is in good agreement with literature reports of 529.3–530.3 eV for oxide, 530.5–531.5 eV for hydroxide, and 531.8–532.8 eV for water,²⁷ which indicates the existence of non-lattice oxygen from water.²⁵

The surface area (A_s) of MnO_2 nanoflowers with short 12 h reaction time (t) (MOF-12) and MnO_2 nanotubes with long 48 h reaction time (MOT-48) were investigated using nitrogen adsorption–desorption isotherms (Fig. 1i). The isotherms were identified as type H3,²⁸ which were characteristic of mesoporous materials, and the Brunauer–Emmett–Teller (BET) specific surface areas for MOF-12 and MOT-48 were 204 and 226 $\text{m}^2 \text{g}^{-1}$, respectively. The pore size distribution of MOF-12 was below 4 nm and that of MOT-48 was at around 8 nm (Fig. S10†), which was in good agreement with the inner diameter measured by HRTEM (Fig. 1g). The N_2 sorption measurement also confirmed that the total pore volume (V_p) and average pore size (d_{av}) of the particles increase with increasing reaction time (Table 1).

To clarify the formation of $\alpha\text{-MnO}_2$ nanotubes and the effect of TBAOH, the reaction without TBAOH was conducted. After 48 h large MnO_2 microflowers were obtained of the rhombohedral phase of $\delta\text{-MnO}_2$ (JCPDS no. 86-666) and no nanotubes were found (Fig. S11 and S12†). Fig. 2 illustrates the formation of $\alpha\text{-MnO}_2$ nanotubes. In this synthesis, $\delta\text{-MnO}_2$ flowerlike particles composed with sheets were first obtained. These sheets were then exfoliated by the effect of the TBAOH, transformed irreversibly into $\alpha\text{-MnO}_2$ tubes, and then connected with other tubes by their ends to form long tubules. For the layered $\delta\text{-MnO}_2$, this consists of 2D edge-shared MnO_6 octahedra layers with K^+ cations and water in the interlayer space. Then, TBA^+ , which enter into the interlayer space and substituted part of the K^+ and water, cause MnO_6 octahedra layers to exfoliate from other layers and form $\alpha\text{-MnO}_2$ nanotubes with 2×2 tunnels by scrolling chiefly in the [001] direction, which was in accord with HRTEM images, accompanied with bond-breaking, re-bonding,

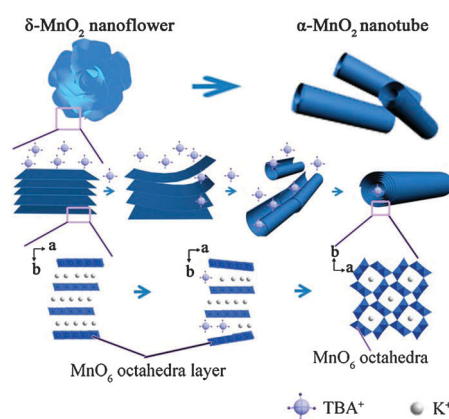


Fig. 2 Scheme of evolution from nanoflower to nanotube MnO_2 via an exfoliation and self-scrolling process.

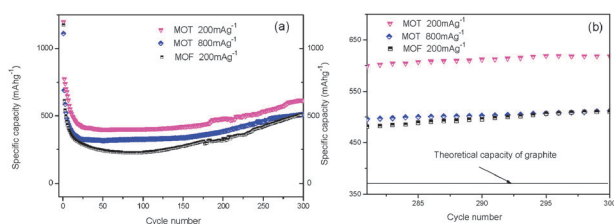


Fig. 3 Variation in discharge capacity vs. (a) cycles and (b) the last 20 cycles of MOT at different current densities of 200 and 800 mA g⁻¹, and that of MOF at a current density of 200 mA g⁻¹.

and new generation of bonds. The tubular conformation allows the anionic surfaces of the sheets to aggregate around TBA⁺, in an entropy-driven process, that leads to the dramatic morphological change and significant increase in the surface area of the nanoparticles.^{22,23}

The electrochemical lithium storage capability of nanotube MnO₂ as potential anode materials for lithium-ion batteries was then evaluated. The charge–discharge voltage profiles of MOT-48 at constant current densities of 200 and 800 mA g⁻¹ and that of MOF-12 at a constant current density of 200 mA g⁻¹ are shown in Fig. S13†, respectively. A distinct voltage plateau at 0.4 V is the typical characteristic of MnO₂.² Fig. 3 shows the cycling performance of MOT and MOF samples. While both MOT and MOF showed a high discharge capacity for the first cycle, MOT exhibited an improved cycling capacity retention compared to MOF and other reported MnO₂ nanoparticles.¹⁷ The irreversible capacity in the first few cycles could be mainly due to the partially irreversible MnO_x conversion reaction with Li, escape of water, and the formation of the solid electrolyte interface (SEI) in the first few lithiation and delithiation cycles.²⁹ Despite these factors, after 50 cycles at a high current density of 800 mA g⁻¹, the phase of MOT was still the tetragonal phase of α-MnO₂, though the morphology of the nanotubes was shortened (Fig. S14†). Fig. 3b shows that the reversible capacity was still stable after hundreds of cycles. After 300 charge–discharge cycles, a reversible capacity of 618 mA h g⁻¹ at a constant current density of 200 mA g⁻¹ can be retained by MOT, which is higher than that of MOF (510 mA h g⁻¹) and the theoretical capacity of graphite of 372 mA h g⁻¹.³⁰ Furthermore, at a high current density of 800 mA g⁻¹ for 300 cycles, a reversible capacity of 512 mA h g⁻¹ can be still retained by MOT. With the similarity in large specific surface area taken into consideration, it is reasonable to attribute the better capacity retention of MOT to its higher degree of mesopore channels and larger total pore volume than that of MOF, 1D nanotube morphology, and its 2 × 2 tunnel structure, which decreased the effective diffusion path and increased the effective space for insertion and extraction of Li.

In summary, α-MnO₂ nanotubes with large surface area were synthesized under hydrothermal conditions *via* an interesting exfoliation and scrolling process. For this process, the addition of TBAOH and the reaction time are important. The as-synthesized α-MnO₂ nanotubes exhibit a high performance at high constant current density for lithium ion batteries, providing reversible capacities of 618 mA h g⁻¹ at a current density of 200 mA g⁻¹ and 512 mA h g⁻¹ at 800 mA g⁻¹

after 300 cycles, respectively. This kind of material will probably have potential applications in chemical power sources, sensors, and other nanodevices.

This work was supported by the State Key Project of Fundamental Research for Nanoscience and Nanotechnology (2011CB932401, 2011CBA00500), and China Postdoctoral Science Foundation (023260007). We are grateful for vice Professor Jiaping Wang and lab assistant Fei Zhao in Tsinghua-Foxconn Nanocenter for their generous help on the fabrication of batteries.

Notes and references

- D. H. Park, S. H. Lee, T. W. Kim, S. T. Lim, S. J. Hwang, Y. S. Yoon, Y. H. Lee and J. H. Choy, *Adv. Funct. Mater.*, 2007, **17**, 2949.
- A. L. M. Reddy, M. M. Shaijumon, S. R. Gowda and P. M. Ajayan, *Nano Lett.*, 2009, **9**, 1002.
- J. Zhao, Z. Tao, J. Liang and J. Chen, *Cryst. Growth Des.*, 2008, **8**, 2799.
- H. Frei and F. Jiao, *Chem. Commun.*, 2010, **46**, 2920.
- J. Desilvestro and O. Haas, *J. Electrochem. Soc.*, 1990, **137**, 5C.
- Y. Cao, L. Xiao, W. Wang, D. Choi, Z. Nie, J. Yu, L. V. Saraf, Z. Yang and J. Liu, *Adv. Mater.*, 2011, **23**, 3155.
- F. Cheng, Z. Tao, J. Liang and J. Chen, *Chem. Mater.*, 2008, **20**, 667.
- J. Luo, H. T. Zhu, H. M. Fan, J. K. Liang, H. L. Shi, G. H. Rao, J. B. Li, Z. M. Du and Z. X. Shen, *J. Phys. Chem. C*, 2008, **112**, 12594.
- T. W. Kim, D. H. Park, S. T. Lim, S. J. Hwang, B. K. Min and J. H. Choy, *Small*, 2008, **4**, 507.
- K. T. Nam, D. W. Kim, P. J. Yoo, C. Y. Chiang, N. Meethong, P. T. Hammond, Y. M. Chiang and A. M. Belcher, *Science*, 2006, **312**, 885.
- M. Wagemaker, A. P. M. Kentgens and F. M. Mulder, *Nature*, 2002, **418**, 397.
- J. Cabana, L. Monconduit, D. Larcher and M. R. Palacin, *Adv. Mater.*, 2010, **22**, E170.
- Z. Wang, D. Luan, F. Y. C. Boey and X. W. Lou, *J. Am. Chem. Soc.*, 2011, **133**, 4738.
- X. Wang and Y. D. Li, *Chem. Lett.*, 2004, **33**, 48.
- X. Wang and Y. Li, *J. Am. Chem. Soc.*, 2002, **124**, 2880.
- X. L. Wiao, L. Wang, D. S. Wang, X. M. He, Q. peng and Y. D. Li, *Nano Res.*, 2010, **2**, 923.
- H. Xia, M. O. Lai and L. Lu, *J. Mater. Chem.*, 2010, **20**, 6896.
- T. X. T. Sayle, R. R. Maphanga, P. E. Ngoepe and D. C. Sayle, *J. Am. Chem. Soc.*, 2009, **131**, 6161.
- Y. Shi, B. Guo, S. A. Corr, Q. Shi, Y.-S. Hu, K. R. Heier, L. Chen, R. Seshadri and G. D. Stucky, *Nano Lett.*, 2009, **9**, 4215.
- S. H. S. Zein, L. C. Yeoh, S. P. Chai, A. R. Mohamed and M. E. M. Mahayuddin, *J. Mater. Process. Technol.*, 2007, **190**, 402.
- W. Chen, Z. L. Fan, L. Gu, X. H. Bao and C. L. Wang, *Chem. Commun.*, 2010, **46**, 3905.
- Y. Kobayashi, H. Hata, M. Salama and T. E. Mallouk, *Nano Lett.*, 2007, **7**, 2142.
- G. B. Saupe, C. C. Waraksa, H. N. Kim, Y. J. Han, D. M. Kaschak, D. M. Skinner and T. E. Mallouk, *Chem. Mater.*, 2000, **12**, 1556.
- D.-W. Wang, F. Li, M. Liu, G. Q. Lu and H.-M. Cheng, *Angew. Chem., Int. Ed.*, 2008, **47**, 373.
- M. K. Yang, J. W. Park, T. K. Ko and J. K. Lee, *Appl. Phys. Lett.*, 2009, **95**.
- J. Ge, L. Zhuo, F. Yang, B. Tang, L. Wu and C. Tung, *J. Phys. Chem. B*, 2006, **110**, 17854.
- D. Yan, P. Yan, S. Cheng, J. Chen, R. Zhuo, J. Feng and G. a. Zhang, *Cryst. Growth Des.*, 2009, **9**, 218.
- K. S. W. Sing, *Pure Appl. Chem.*, 1982, **54**, 2201.
- J. Guo, Q. Liu, C. Wang and M. R. Zachariah, *Adv. Funct. Mater.*, 2012, **22**, 803.
- J. S. Chen, T. Zhu, X. H. Yang, H. G. Yang and X. W. Lou, *J. Am. Chem. Soc.*, 2010, **132**, 13162.